

# Surface-roughness restricts families of exact coherent structures in wall-bounded flows

Sabarish Vadarevu,<sup>\*</sup> Ati Sharma,<sup>†</sup> and Bharathram Ganapathisubramani<sup>‡</sup>  
*University of Southampton*  
 (Dated: November 23, 2018)

Recent progress indicates that highly symmetric recurring solutions of the Navier-Stokes equations such as equilibria and periodic orbits provide a skeleton for turbulence dynamics in state-space. Many of these solutions have been found for smooth-walled plane Couette, channel, and pipe flows. Rough-walled flows are of great practical significance, yet no recurring solutions are known for these flows. We present a numerical homotopy method to continue solutions from smooth-walled flows to corresponding rough-walled flows, illustrated here for grooved Couette flow at a Reynolds number of 400. Loss of spanwise homogeneity reduces continuous families of solutions (identical up to translational shifts) in smooth Couette flow to multiple, discrete families in grooved Couette flow. The discrete families are ones that can preserve the discrete symmetries of Couette flow. Continuation of these solutions suggests that the exact coherent structures of smooth-walled flows also dominate rough-walled flows. Reduction of continuous families to discrete families implies that turbulence statistics in grooved Couette flow, and rough-walled flows by extension, must retain the spatial variation of exact solutions. These results raise important questions concerning the role of symmetries in understanding rough-walled turbulence.

*Introduction.*— For most of the 20th century, turbulence was studied through the lens of statistics despite knowledge of the existence of certain recurring structures. Townsend’s attached eddy hypothesis [1] was an early attempt to describe turbulence in terms of coherent structures and relate their scaling to observed statistics. These eddies were suspected to be the building blocks of turbulence [2], but they were ad-hoc structures without basis in the Navier-Stokes equations (NSE). Advances in computational power allowed computation of so-called exact coherent structures, starting with plane Couette flow (PCF) equilibria of Nagata [3]. Similar solutions were found at asymptotically high Reynolds numbers by Hall and Smith [4] highlighting the inviscid mechanism of vortex-wave interactions [5]. Minimal channel DNS of Jiménez and Moin [6] confirmed the significance of the interaction between streamwise streaks and vortices seen in the equilibria. Waleffe [7] provided a detailed picture of the recurring motions that occur in wall-bounded turbulence; the linear instability and non-linear breakdown of streaks produces vortices, which in turn feed into the streaks. In the past several years, many exact solutions of the Navier Stokes equations have been found and their connections in state-space have been mapped (for instance, [8–12]). Today, these solutions — equilibria, travelling waves, periodic orbits, and relative periodic orbits — are understood to form a skeleton for turbulent trajectories in state-space.

While rapid progress has been made towards understanding turbulence dynamics in terms of exact recurrent solutions of the NSE, such efforts are yet to involve wall-roughness, despite the practical significance of rough-walled turbulence. Studying the variation in the structure and statistics of exact solutions with changing wall geometry (from smooth to rough) can offer insight into the interactions of wall-roughness with turbulent flow. This approach will complement the work to

date on rough-walled turbulence [13–15], where turbulence structure and statistics are examined using experimental and numerical methods, to provide a quantitative basis for characterizing surface topologies and relating them to measures such as equivalent sand roughness. Drag reduction observed in riblet-mounted boundary layers [16, 17] is of special interest, and we find that this can be explained by the restriction of exact coherent structures by grooves.

The original solutions of Nagata [3] were obtained using homotopy from Taylor-Vortex flow to PCF. We use homotopy to extend solutions from smooth-walled flows to rough-walled flows using a domain transformation method, illustrated in this letter for grooved PCF by extending both equilibria of Nagata [3]. Smooth PCF has streamwise and spanwise homogeneity. A consequence of this is that each equilibrium inhabits a family of solutions that are identical in structure but differ by a translational shift in the streamwise and/or spanwise directions. Of a family of such solutions, we find that only some solutions with a certain phase relative to the grooves can continue to grooved PCF. The continuous translational symmetry of grooved PCF gives way to a discrete symmetry in grooved PCF. We also see that, while the solutions that can continue to grooved PCF retain the structure of streamwise streaks and streamwise vortices, the structures get distorted as groove amplitude increases. Our results also support the mechanism for drag reduction observed in riblet-mounted boundary layers [18].

*Methodology.*— We study incompressible plane Couette flow using non-dimensional coordinates  $(x, y, z)$  along the streamwise, wall-normal, and spanwise directions respectively, non-dimensionalized by half of the distance between the walls. A Fourier series is used to represent roughness. A general case of wall roughness periodic

in  $(L_x, L_z) = (2\pi/\alpha, 2\pi/\beta)$  can be represented by

$$\begin{aligned} y_{top} &= 1 + \sum_{l,m} A_{l,m}^t e^{i(l\alpha x + m\beta z + \phi_{l,m}^t)}, \\ y_{bottom} &= -1 + \sum_{l,m} A_{l,m}^b e^{i(l\alpha x + m\beta z + \phi_{l,m}^b)}. \end{aligned} \quad (1)$$

*Domain transformation.*— We wish to map this geometry to a flat-walled geometry using a domain transformation,  $Y = -1 + 2(y - y_{bottom})/(y_{top} - y_{bottom})$  (for similar usage, see [19, 20]). The Fourier spectral method is easily applied in the transformed domain, but mapping partial derivatives from the transformed domain to the physical domain of eq. (1) is rather cumbersome. However, when  $A_{l,m}^t = A_{l,m}^b$  and  $\phi_{l,m}^t = \phi_{l,m}^b$ , i.e., when the width between the top and bottom walls remains constant, the required domain transformation is

$$Y = y - \sum_{l,m} A_{l,m} e^{i(l\alpha x + m\beta z + \phi_{l,m})}, \quad (2)$$

which produces simpler relations between the partial derivatives in the physical domain of eq. (1) and the transformed domain.

*Grooved PCF.*— In this letter, we investigate the special case of longitudinal grooves ( $\alpha = 0$ ), with the additional simplification that  $\phi_m = 0$ . The top and bottom walls of the PCF are given by

$$y_{walls} = \pm 1 + \sum_m A_m \cos(m\beta z), \quad (3)$$

and the grooved PCF is mapped to a smooth PCF geometry as

$$\begin{aligned} X &= x, \\ Y &= T(y, z) = y - \sum_m A_m \cos(m\beta z), \\ Z &= z. \end{aligned} \quad (4)$$

The partial derivatives in the two domains relate as

$$\begin{aligned} \partial_x &= \partial_X, \\ \partial_y &= \partial_Y, \\ \partial_z &= \partial_Z + \left( \sum_m m\beta A_m \sin(m\beta z) \right) \partial_Y. \end{aligned} \quad (5)$$

*Numerical method.*— A primitive variable formulation is used in a steady-state solver to extend the equilibria of Nagata [3] to grooved PCF. The velocities ( $u, v, w$  along  $x, y, z$ ) are non-dimensionalized by the speed of the walls, and the pressure is non-dimensionalized by  $\rho U_{walls}^2$ . The equations to be solved are

$$\begin{aligned} u\partial_x u + v\partial_y u + w\partial_z u + \partial_x p - \frac{1}{Re}\Delta u &= 0, \\ u\partial_x v + v\partial_y v + w\partial_z v + \partial_y p - \frac{1}{Re}\Delta v &= 0, \\ u\partial_x w + v\partial_y w + w\partial_z w + \partial_z p - \frac{1}{Re}\Delta w &= 0, \\ \partial_x u + \partial_y v + \partial_z w &= 0, \end{aligned} \quad (6)$$

with the boundary conditions

$$\begin{aligned} u(y = y_{top}) &= 1, & u(y = y_{bottom}) &= -1, \\ v(y = y_{walls}) &= 0, & w(y = y_{walls}) &= 0, \\ \{\nabla \cdot \mathbf{u}\}(y = y_{walls}) &= 0. \end{aligned} \quad (7)$$

The Reynolds number  $Re$  is based on the dimensional half-width and the dimensional speed of the walls.

The velocities and pressure are mapped from the grooved PCF domain with walls given in eq. (3) to a smooth PCF domain according to eq. (4); the boundary conditions in the transformed domain are

$$\begin{aligned} u(Y = \pm 1) &= \pm 1, & v(Y = \pm 1) &= 0, \\ w(Y = \pm 1) &= \pm 1, & \{\nabla \cdot \mathbf{u}\}(Y = \pm 1) &= 0 \end{aligned} \quad (8)$$

The fields are discretized using the Fourier method along the streamwise and spanwise directions and the Chebyshev collocation method along the wall-normal direction in the transformed domain  $(X, Y, Z)$ . Equation (6) are discretized by writing the partial derivatives in  $x, y, z$  in terms of partial derivatives in  $X, Y, Z$  using eq. (5). A major consequence of the domain transformation is that the Fourier coefficients of the spanwise derivatives involve multiple Fourier modes:

$$\begin{aligned} \{\partial_x u\}_{l,m} &= il\alpha u_{l,m}, \\ \{\partial_y u\}_{l,m} &= \partial_Y(u_{l,m}), \\ \{\partial_z u\}_{l,m} &= im\beta u_{l,m} + \frac{-i\beta}{2} \sum_q q A_q u_{l,m-q}, \end{aligned} \quad (9)$$

where  $u_{l,m}$  is the  $Y$ -dependent Fourier coefficient for mode  $(l\alpha, m\beta)$ . This additional inter-modal interaction contains all the information due to the grooved walls, and is the trade-off for the simplified boundary conditions of eq. (8).

The discretized equations are solved using the Newton-Raphson method. A full-rank matrix inversion (SVD-based) is used in the iterative correction steps. The iterations are initialized with exact solutions for smooth PCF, EQ1 (lower branch) and EQ2 (upper branch) of Nagata [3] taken from the solutions database of Gibson [21]. Our steady-state solver defines instantaneous time-derivatives of the velocity fields as the residual ( $\mathbf{r}$ ), and the residual norm is defined as the integral

$$\|\mathbf{r}\| = \left[ \int_{x=0}^{2\pi/\alpha} \int_{z=0}^{2\pi/\beta} \int_{y=y_{bottom}}^{y_{top}} (\dot{u}^2 + \dot{v}^2 + \dot{w}^2) dy dz dx \right]^{1/2}. \quad (10)$$

Solutions for grooved PCF are computed with 35 wall-normal Chebyshev nodes and 825 Fourier modes:  $|l| \leq 14$  and  $|m| \leq 16$  along the streamwise and spanwise directions respectively. Accuracy of the solutions is defined as the residual norm of the solutions when extrapolated on a grid with 70 Chebyshev nodes and 3185 Fourier modes:  $|l| \leq 28$  and  $|m| \leq 32$ . This definition differs

from conventional definitions that involve time-marching at increased resolution because of the steady-state solver used here.

*Results.*— We present results for the “one-groove-per-box” case with  $A_q = 0 \quad \forall q \neq 1$ , illustrated in fig. 1.

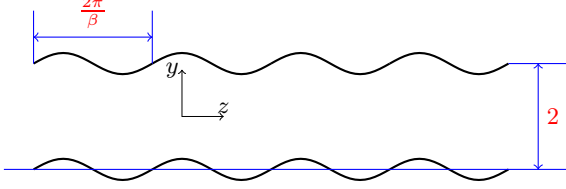


FIG. 1: Cross-stream slice of grooved PCF geometry; “One groove per box”:  $A_1 = 0.1$

The wavelength of the grooves, defined by ( $L_z = 2\pi/\beta$ ), is set to coincide with the spanwise periodic length of the solutions we wish to continue:  $\beta = 2.5$ . The streamwise length of the periodic box is also set according to the solutions to be continued,  $\alpha = 1.14$ . All solutions are for  $Re = 400$ . The smooth PCF solutions EQ1 (lower branch) and EQ2 (upper branch) are shown in figs. 2a and 2b; contours of streamwise velocity and quiver arrows for cross-stream velocities are plotted. The continued solutions for grooved PCF are shown in figs. 2c and 2d at  $A_1 = 10\%$ . The vortex-streak interaction in grooved PCF can be seen from the isosurfaces of zero streamwise velocity and  $\pm 0.7\max(\omega_x)$  streamwise vorticity.

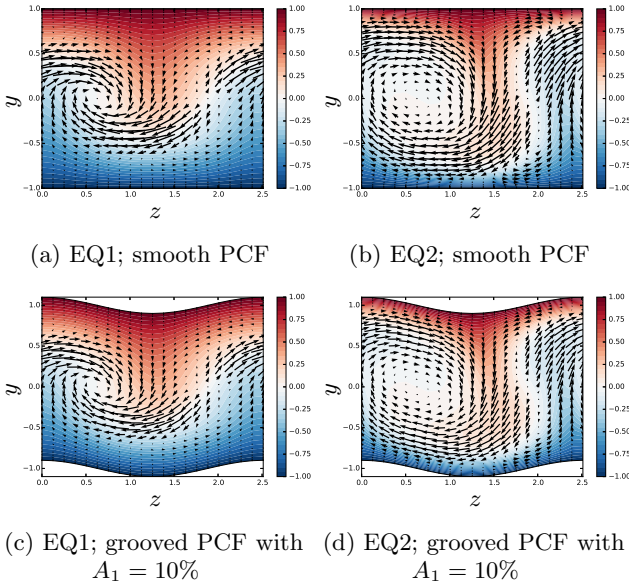


FIG. 2: Velocity on a cross-stream plane ( $x = 0$ ) for smooth PCF (a-b) and grooved PCF (c-d). Contours show streamwise velocity and quiver arrows show cross-stream velocities.

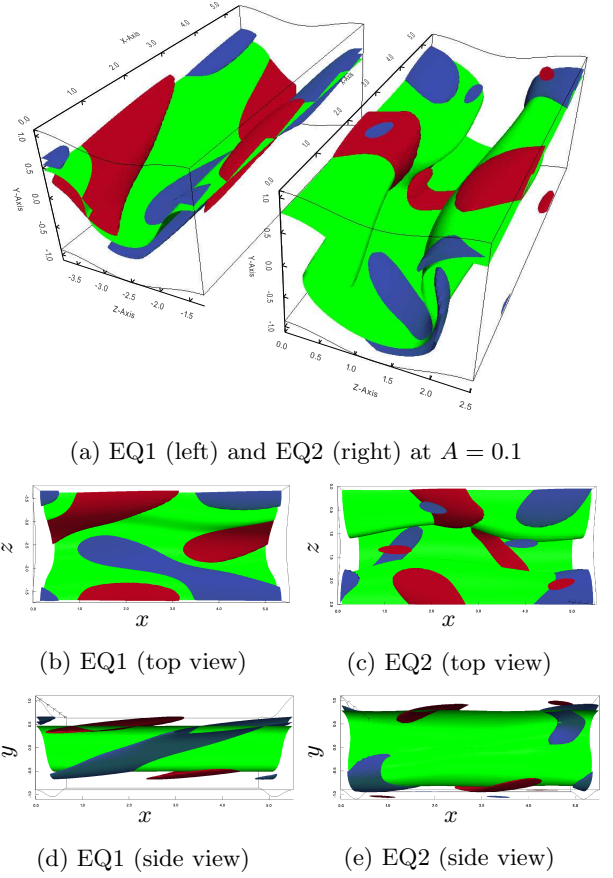


FIG. 3: Lower (EQ1) and upper (EQ2) branch equilibria for grooved PCF at  $A = 0.1$  showing isosurfaces for zero streamwise velocity (green) and streamwise vortices for  $\omega_x = 0.7\max(\omega_x)$  (red) and  $-0.7\max(\omega_x)$  (blue).

ity shown in fig. 3. The residual norm for these solutions is lower than  $10^{-12}$  and their accuracy is  $\sim 10^{-5}$ .

Solutions for grooved PCF look similar to their smooth PCF counterparts, except for some distortion in the streamwise vortices. In fact, the flowfields for grooved PCF solutions have  $\approx 99\%$  energy in the smooth PCF solution-structure when projected on the latter in the transformed domain  $(X, Y, Z)$ .

*Structure.*— The equilibria of grooved PCF retain the structure of their smooth PCF counterparts. Streamwise streaks are accompanied by streamwise vortices centered on the low speed streaks. This is not surprising; the interaction of streamwise streaks and vortices is known to exist irrespective of the kind of wall-bounded flow [7, 22]. So, the action of the grooves on the structure of EQ1 and EQ2 shown in figs. 2a and 2b is to distort the cross-stream flow.

*Phase-restriction.*— However, the flowfield shown in fig. 2a is just one member of a continuous family of solu-

tions that arise due to spanwise homogeneity of smooth PCF. Let this particular member be called  $\chi^*$ . Let us denote a flowfield that is obtained by translating  $\chi^*$  along  $z$  by some shift  $l_z$  as  $S_{l_z}(\chi^*)$ . The Fourier coefficients, denoted  $\mathcal{F}\{\cdot\}_{k,m}$  for mode  $e^{i(k\alpha X + m\beta Z)}$ , of  $S_{l_z}(\chi^*)$  can be related to the Fourier coefficients of  $\chi^*$  as

$$\mathcal{F}\{S_{l_z}(\chi^*)\}_{k,m}(Y) = e^{-2\pi i m(l_z/L_z)} \mathcal{F}\{\chi^*\}_{k,m}(Y), \quad (11)$$

so that spanwise translation of flowfields can be seen as phase-shifts in the Fourier coefficients.

Let us also define the continuous family of flowfields obtained by translating  $\chi^*$  along  $z$  as  $\tilde{\mathcal{F}}(\chi^*) = \{S_{\delta z}(\chi^*) : \delta z \in \mathbb{R}\}$ , and the discrete family of flowfields obtained by translating  $\chi^*$  along  $z$  through integral multiples of  $L_z/n$  as  $\mathcal{F}_n(\chi^*) = \{S_{qL_z/n}(\chi^*) : q \in \mathbb{Z}\}$ . The argument  $\chi^*$  for  $\mathcal{F}$  is dropped for convenience. Every  $\mathcal{F}_n$  is a subset of  $\tilde{\mathcal{F}}$ . The members of  $\mathcal{F}_1$  are identical to each other due to the periodicity of  $\chi^*$ .

For smooth PCF, because of its spanwise homogeneity, every member of  $\tilde{\mathcal{F}}$  is an equilibrium of the NSE. When  $\chi^*$  is used as the initial iterate for finding a grooved PCF equilibrium with groove amplitude  $A$ , it converges to  $\chi_A^*$ . However, when a different member of  $\tilde{\mathcal{F}}$  is used as the initial iterate, convergence is not likely. We find that the iterations converge only for flowfields  $\chi \in \mathcal{F}_2$ , or for flowfields sufficiently close to members of  $\mathcal{F}_2$ ; the converged solutions for the latter case are identical to the solutions obtained from continuing the corresponding member in  $\mathcal{F}_2$ . Failure of iterations to converge indicates that the initial iterate is not in the vicinity of an equilibrium. We take this as indicating that most members of  $\tilde{\mathcal{F}}$  do not have a corresponding equilibrium in grooved PCF.

*Discrete symmetries.*— The special significance of  $\mathcal{F}_2$  can be attributed to a discrete symmetry of PCF. Certain discrete symmetries are known to be important to exact recurring solutions of the NSE [8]. The original equilibria, EQ1 and EQ2, are invariant under one such symmetry; the shift-reflect symmetry given by

$$s_1[u, v, w](x, y, z) = [u, v, -w](x + L_x/2, y, -z), \quad (12)$$

which is a composition of reflection along the  $x - y$  plane  $z = 0$  and a half-cell shift along  $x$ ; the reflection and  $x$ -shift commute. Because of the spanwise homogeneity of smooth PCF, it admits solutions with reflectional symmetry about any  $x - y$  plane, such as a flowfield  $\chi = S_{l_z}(\chi^*)$  which is shift-reflect invariant about the plane  $z = l_z$ . By contrast, grooved PCF has reflectional symmetry only about particular  $x - y$  planes, as can be seen in fig. 1. In  $[0, 2\pi/\beta)$ , reflectional symmetry holds only for planes  $z = 0$  and  $z = \pi/\beta$ . So, any equilibrium of grooved PCF can have reflectional symmetry only about these two planes. Initial iterates from  $\mathcal{F}_2$  conform to this symmetry even if they do not exactly satisfy the NSE, while flowfields in  $\tilde{\mathcal{F}} - \mathcal{F}_2$  do not even satisfy the symmetry. Our results show that the solutions obtained by

continuing  $\mathcal{F}_2$  also satisfy the shift-reflect symmetry of eq. (12).

*Bifurcation.*—  $\mathcal{F}_2$  has two distinct members,  $\chi^*$  and  $S_{L_z/2}(\chi^*)$ , denoted  $\chi^+$ . Let us denote their continued solutions at some amplitude  $A$  by  $\chi_A^*$  and  $\chi_A^+$  respectively. Our results show that  $\chi_A^+ \neq S_{L_z/2}(\chi_A^*)$ ; the members of  $\mathcal{F}_2(\chi^*)$  bifurcate into two distinct families of solutions in grooved PCF:  $\mathcal{F}_1(\chi_A^*)$  and  $\mathcal{F}_1(\chi_A^+)$ , with distinct values for scalars such as energy density and bulk dissipation rate. The difference arises because, while grooved PCF has reflectional symmetry about both  $z = 0$  and  $z = \pi/\beta$ , the walls at  $z = 0$  are displaced along  $+y$  and the walls at  $z = \pi/\beta$  are displaced along  $-y$ . This bifurcation can also be interpreted in terms of continuing  $\chi^*$  along positive and negative groove amplitudes.

*Localization.*— Willis *et al.* [23] argue that the presence of continuous families of solutions could obscure our description of turbulent flow and describe a method of slices to systematically reduce a family of similar solutions to one representative solution; with this approach, travelling wave solutions reduce to equilibria, and relative periodic orbits to periodic orbits. Grooved PCF achieves this reduction by physically disrupting some of these symmetries. Spatially localized equilibria have also been found in smooth PCF [24, 25]. Based on our results for global solutions, we can expect that any symmetric localized solutions, when extended to grooved PCF, would also be phase-restricted by the grooves.

In smooth PCF turbulence, any of the solutions in a family  $\tilde{\mathcal{F}}$  could be visited; no member of a family is special. As a result, turbulence statistics would only show spatial averages over an entire family of solutions. The phase-restriction of solutions in grooved PCF, however, implies that turbulence statistics should reflect the spatial structure of the solutions.

*Riblets.*— Certain geometries of riblets in boundary layer flows produce a reduction in drag [16, 18, 26]. The drag reduction in such flows is explained as due to streamwise vortices that sit on top of riblets, sustaining low-speed streaks within riblet-valleys which produce lower drag (by  $\sim 8\% - 16\%$ ) than in smooth-walled flows [18]. The reduction of continuous families of solutions to discrete families by grooved PCF due to symmetry preservation supports this description of riblet-mounted flows. We can reasonably suppose that, in addition to anchoring exact coherent structures spatially, grooves also filter out near-wall coherent structures whose size does not match that of the grooves; this can be exploited in the future to design geometries that specifically filter out coherent structures with the greatest contribution to turbulent drag.

*Conclusion and outlook.*— The presence of grooves produces two effects: distortion of the exact structures, and reduction of continuous solution-families (of dynamically similar solutions identical up to a translation) to multiple, discrete solution-families defined by a phase re-



striction due to grooves. The latter effect is attributed to preservation of a shift-reflect symmetry of PCF, and produces two distinct discrete families for positive and negative groove amplitudes. This phase restriction supports the proposed mechanism for drag reduction in riblet-mounted boundary layers.

Our discussion thus far has only focused on extending symmetric solutions to PCF with symmetric grooves. This led us to discover the phase restriction and spatial anchoring of exact coherent structures. This raises several interesting questions, such as: Does the reduction of continuous families to discrete families hold for PCF with asymmetric grooves? How do asymmetric solutions of smooth PCF continue to symmetric grooved PCF? What is the significance of distortion of coherent structures by the grooves? How well can weighted averaging over such discrete solution-families predict drag due to roughness? We believe that answering these questions can lead us to a comprehensive understanding of the dynamics of rough-walled turbulence in the near future.

*Acknowledgement.*— The authors acknowledge the use of the IRIDIS High Performance Computing Facility, and associated support services at the University of Southampton, in the completion of this work.

---

\* sbv1g13@soton.ac.uk

† A.Sharma@soton.ac.uk; <http://www.atisharma.info>

‡ G.Bharath@soton.ac.uk; <http://www.bharath-lab.org/>

- [1] A. A. Townsend, *The structure of turbulent shear flow* (Cambridge university press, 1980).
- [2] A. Perry and I. Marušić, *Journal of Fluid Mechanics* **298**, 361 (1995).
- [3] M. Nagata, *Journal of Fluid Mechanics* **217**, 519 (1990).
- [4] P. Hall and F. T. Smith, *Journal of fluid mechanics* **227**, 641 (1991).
- [5] P. Hall and S. Sherwin, *Journal of Fluid Mechanics* **661**, 178 (2010).
- [6] J. Jiménez and P. Moin, *Journal of Fluid Mechanics* **225**, 213 (1991).
- [7] F. Waleffe, *Physics of Fluids* (1994-present) **9**, 883 (1997).
- [8] J. F. Gibson, J. Halcrow, and P. Cvitanović, *Journal of Fluid Mechanics* **611**, 107 (2008).
- [9] B. Eckhardt, H. Faisst, A. Schmieg, and T. M. Schneider, *Philosophical Transactions of the Royal Society of London A: Mathematical, Physical and Engineering Sciences* **366**, 1297 (2008).
- [10] G. Kawahara, M. Uhlmann, and L. van Veen, *Annual Review of Fluid Mechanics* **44**, 203 (2012).
- [11] J. S. Park and M. D. Graham, *Journal of Fluid Mechanics* **782**, 430 (2015).
- [12] A. P. Willis, K. Y. Short, and P. Cvitanović, *arXiv preprint arXiv:1504.05825* (2015).
- [13] J. Jiménez, *Annual Review of Fluid Mechanics* **36**, 173 (2004).
- [14] K. A. Flack and M. P. Schultz, *Physics of Fluids* (1994-present) **26**, 101305 (2014).
- [15] D. Squire, C. Morrill-Winter, N. Hutchins, M. Schultz, J. Klewicki, and I. Marusic, *Journal of Fluid Mechanics* **795**, 210 (2016).
- [16] M. J. Walsh, *Journal of Aircraft* **27**, 572 (1990).
- [17] A. Bannier, E. Garnier, and P. Sagaut, in *Progress in Wall Turbulence 2* (Springer, 2016) pp. 213–224.
- [18] B. Dean and B. Bhushan, *Philosophical Transactions of the Royal Society of London A: Mathematical, Physical and Engineering Sciences* **368**, 4775 (2010).
- [19] A. Kasliwal, S. Duncan, and A. Papachristodoulou, in *Control (CONTROL), 2012 UKACC International Conference on* (IEEE, 2012) pp. 625–630.
- [20] H. V. Moradi and J. M. Floryan, *International Journal of Heat and Mass Transfer* **66**, 517 (2013).
- [21] J. F. Gibson, *Channelflow: A spectral Navier-Stokes simulator in C++*, Tech. Rep. (U. New Hampshire, 2014) [Channelflow.org](http://Channelflow.org).
- [22] H. Blackburn, P. Hall, and S. Sherwin, *Journal of Fluid Mechanics* **726**, R2 (2013).
- [23] A. P. Willis, P. Cvitanović, and M. Avila, *Journal of Fluid Mechanics* **721**, 514 (2013).
- [24] J. Gibson and E. Brand, *Journal of Fluid Mechanics* **745**, 25 (2014).
- [25] M. Chantry and R. R. Kerswell, *Physical Review E* **91**, 043005 (2015).
- [26] I. TANI, *Proceedings of the Japan Academy. Ser. B: Physical and Biological Sciences* **64**, 21 (1988).